JOURNAL OF NATURAL PRODUCTS

pubs.acs.org/jnp

Article

Bifunctional Doscadenamides Activate Quorum Sensing in Gram-Negative Bacteria and Synergize with TRAIL to Induce Apoptosis in Cancer Cells

Xiao Liang, Qi-Yin Chen, Gustavo M. Seabra, Susan Matthew, Jason C. Kwan, Chenglong Li, Valerie J. Paul, and Hendrik Luesch*

Cite This: *J. Nat. Prod.* 2021, 84, 779−789

Read Online

ACCESS | Metrics & More | Article Recommendations | Supporting Information

ABSTRACT: New cyanobacteria-derived bifunctional analogues of doscadenamide A, a LasR-dependent quorum sensing (QS) activator in *Pseudomonas aeruginosa*, characterized by dual acylation of the pyrrolinone core structure and the pendant side chain primary amine to form an imide/amide hybrid are reported. The identities of doscadenamides B−J were confirmed through total synthesis and a strategic focused library with different acylation and unsaturation patterns was created. Key molecular interactions for binding with LasR and a functional response through mutation studies coupled with molecular docking were identified. The structure−activity relationships (SARs) were probed in various Gram-negative bacteria, including *P. aeruginosa* and *Vibrio harveyi*, indicating that the pyrrolinone-N acyl chain is critical for full agonist activity, while the other acyl chain is dispensable or can result in antagonist activity, depending on the bacterial system. Since homoserine lactone (HSL) quorum sensing activators have been shown to act in synergy with TRAIL to induce apoptosis in cancer cells, selected doscadenamides were tested in orthogonal eukaryotic screening systems. The most potent QS agonists, doscadenamides S10−S12, along with doscadenamides F and S4 with partial or complete saturation of the acyl side chains, exhibited the most pronounced synergistic effects with TRAIL in triple negative MDA-MB-231 breast cancer cells. The overall correlation of the SAR with respect to prokaryotic and eukaryotic targets may hint at coevolutionary processes and intriguing host−bacteria relationships. The doscadenamide scaffold represents a non-HSL template for combination therapy with TRAIL pathway stimulators.

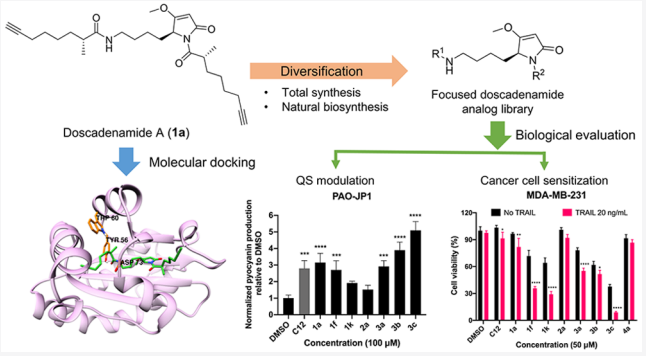

The tumor necrosis factor-related apoptosis-inducing ligand (TRAIL), also known as Apo-2L and TNFSF10, is a TNF family cytokine that can induce cell apoptosis and cause programmed cell death by binding to the death receptors DR4 (TRAIL-RI) and DR5 (TRAIL-RII).[1,2] Moreover, there are studies showing that TRAIL can selectively cause cancer cell death without detrimental effects on normal cells.[2,3] This selectivity has made TRAIL a promising candidate for cancer therapy[4] and stimulated intensive studies toward the development of therapeutic agents targeting the TRAIL signaling pathway,[1] including recombinant TRAIL proteins and monoclonal antibody agonists specific for DR4 (TRAIL-RI) and DR5 (TRAIL-RII).[5] However, these agents did not achieve satisfying anticancer activities in clinical investigations,[6] because many cancer cells have developed resistance toward TRAIL, thus compromising the efficacy of TRAIL-therapy.[4,7]

Previously, the bacterial quorum sensing (QS) activator *N*-(3-oxododecanoyl)-L-homoserine lactone (C12) was reported to enhance the TRAIL-induced apoptosis in cancer cells, thus sensitizing the cells to TRAIL therapy.[7] Recently, we have isolated and reported a new QS activator, doscadenamide A[8] (**1a**, Figure 1), from the cyanobacterium *Moorena bouillonii* collected at Finger Reef, Guam.[9] Doscadenamide A (**1a**) possesses an unique structural skeleton featuring a pyrrolinone core with a pendant side chain linker (*py*Lys-OMe), and this core structure is doubly acylated with the same carboxylic acid, (*R*)-2-methyl-oct-7-ynoic acid (Moya), (1) on the side chain amine (Moya1) and (2) the five-membered amide ring structure (Moya2), to form amides and imides, respectively (Figure 1).[9] Our initial investigation indicated that doscadenamide A (**1a**) is an unprecedented nonhomoserine lactone

Special Issue: Special Issue in Honor of A. Douglas Kinghorn

Received: September 14, 2020
Published: January 22, 2021

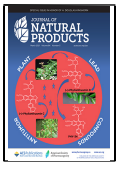

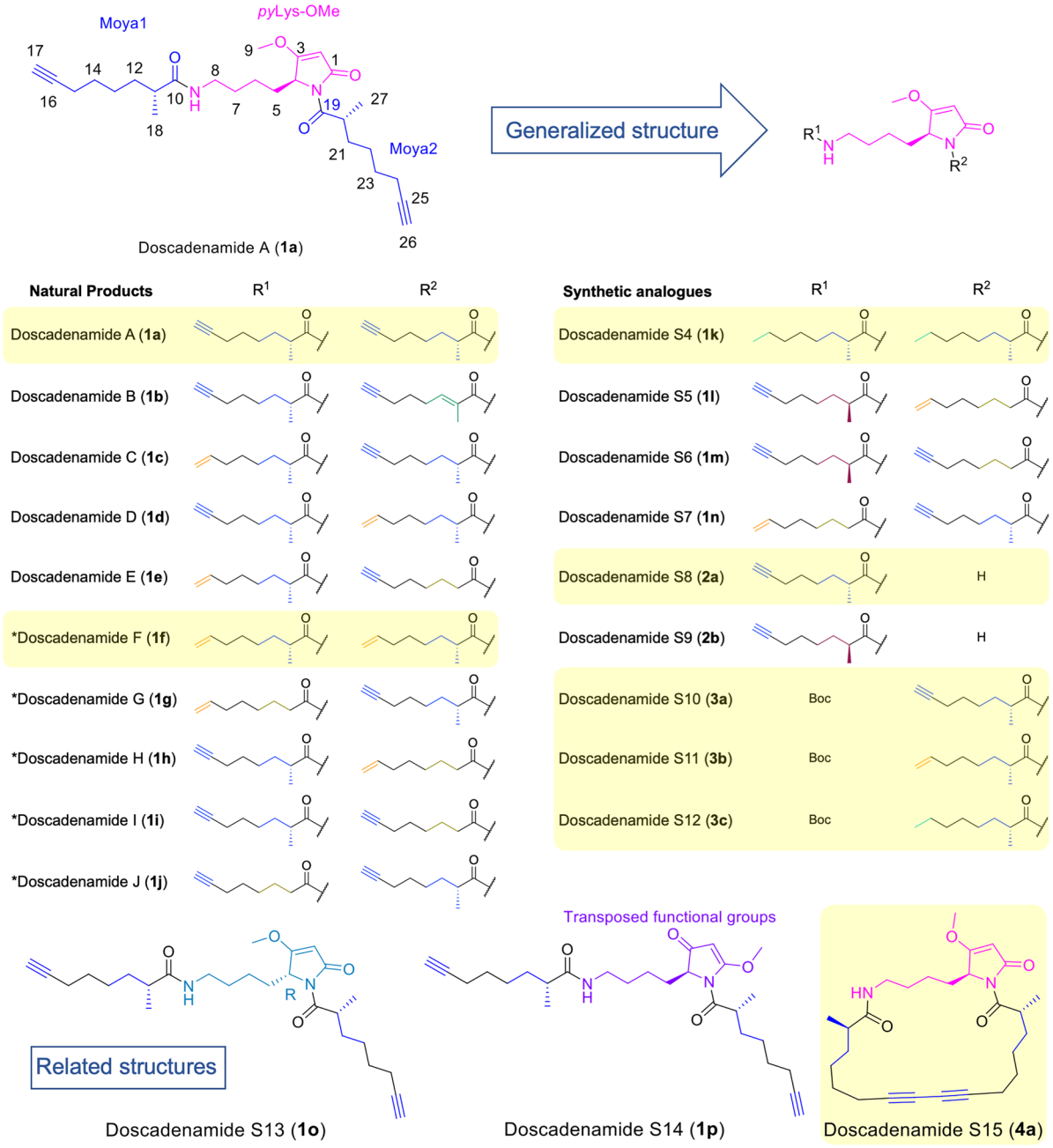

Figure 1. Structures of doscadenamides, including naturally occurring doscadenamides and synthetic structural analogues of doscadenamide A. The core structure/general skeleton is diversified through different acylation patterns. Additional structures are characterized by inversion of the pyrrolinone ring configuration, transposed pyrrolinone functional groups or cyclization. Compounds included in the SAR study described in this manuscript are highlighted in yellow. *Natural products that were synthesized.

(HSL) QS agonist that is able to activate the QS signaling pathway in *Pseudomonas aeruginosa* in a LasR dependent manner.[9] LasR is a transcriptional activator of *Pseudomonas aeruginosa* virulence genes and belongs to the LuxR protein family that was named after the regulator of bioluminescence (*lux*) in *Vibrio fischeri*.[10,11]

Here we describe the identification of additional natural doscadenamides (B–I) from the same cyanobacterium and the synthesis of strategically diversified analogues to probe the structure–activity relationship (SAR) with respect to QS modulation in several different Gram-negative bacterial systems and interrogated the tentatively causative molecular interactions with bacterial receptors. We then evaluated a subset of the focused doscadenamide library in cancer cells and successfully established a synergistic activity with TRAIL in invasive triple negative breast cancer cells.

RESULTS

Isolation and Characterization of Natural Doscadenamides B–J. The isolation of doscadenamide A (**1a**, Figure 1) from *M. bouillonii* was reported previously.[9] A chemical investigation of the original extracts enabled the identification of several related compounds that differed in the degree of unsaturation and methylation pattern (Figure 1). 1D and 2D NMR analysis (Tables S1–S7) coupled with high resolution electrospray ionization mass spectrometry (HRESIMS) and

https://dx.doi.org/10.1021/acs.jnatprod.0c01003
J. Nat. Prod. 2021, 84, 779–789

Scheme 1. Total Synthesis of Doscadenamide H (1h)

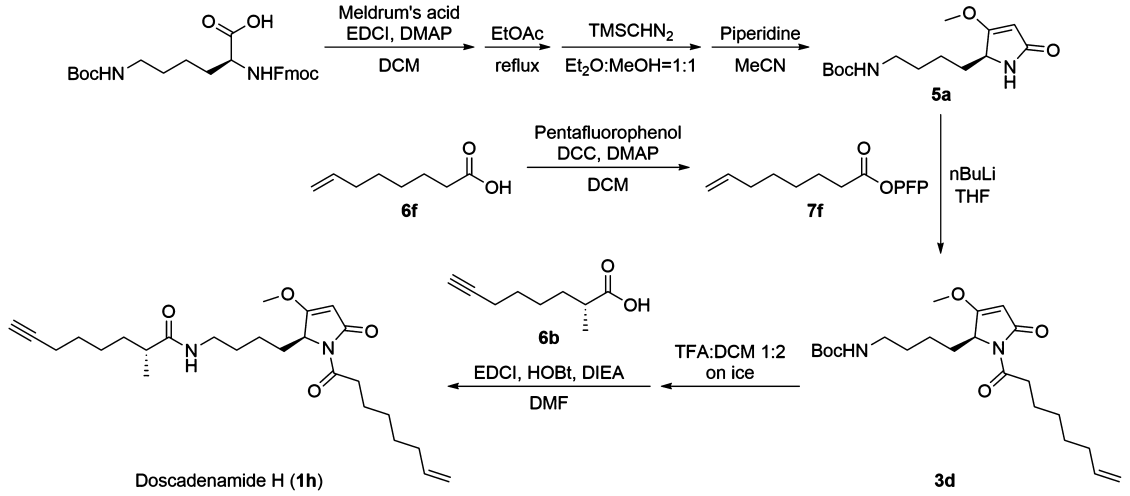

synthesis of selected family members unambiguously established the structures.

Briefly, we isolated five pure structural analogues, doscadenamides B−F (**1b**−**1f**, Figures 1 and S1−28, Tables S1−5) as well as impure doscadenamides G−J (**1g**−**j**, Figures 1 and S29−31, Tables S6−7). Doscadenamide B (**1b**, Figure 1) features an alkene moiety in the R^2 side chain. The HRESIMS spectrum of **1b** in positive mode exhibited a $[M + H]^+$ peak at m/z 455.2897 with ten degrees of unsaturation; while the ^{1}H NMR spectrum of **1b** in $CDCl_3$ further confirmed the presence of characteristic signals corresponding to the alkene proton (δ_H 5.94 ppm) and the attached methyl group (δ_H 1.90 ppm) (Figures S1−6, Table S1). Doscadenamide C (**1c**, Figure 1) and doscadenamide D (**1d**, Figure 1) feature a vinyl terminus at R^1 and R^2 side chain, respectively. The HRESIMS spectrum of **1c** and **1d** in positive mode exhibited a $[M + H]^+$ peak at m/z 459.3218 and m/z 459.3226 with eight degrees of unsaturation, while the ^{1}H NMR spectrum of **1c** and **1d** in $CDCl_3$ suggested the presence of a vinyl group at 4.96 and 4.94 ppm, respectively (Figures S7−17, Tables S2−3). Doscadenamide E (**1e**, Figure 1) not only features a vinyl terminus at the R^1 side chain but also exhibits the loss of the α-methyl group compared to doscadenamide A (**1a**, Figure 1). The HRESIMS spectrum of **1e** in positive mode exhibited a $[M + H]^+$ peak at m/z 445.3069 with eight degrees of unsaturation, and the ^{1}H NMR spectrum of **1e** in $CDCl_3$ indicated the characteristic signals of a vinyl group at 4.96 ppm and methylene at 2.94 ppm (Figures S18−22, Table S4). Doscadenamide F (**1f**, Figure 1) possesses two vinyl termini, which was supported by its HRESIMS spectrum in the positive mode showing a $[M + H]^+$ peak at m/z 461.3362 with seven degrees of unsaturation and its ^{1}H NMR spectrum in $CDCl_3$ at 4.95 and 4.97 ppm for characteristic signals of vinyl groups (Figure 23−28, Table S5). Doscadenamide G (**1g**, Figure 1) includes a R^1 side chain with a vinyl terminus without α-methylation, while doscadenamide H (**1h**, Figure 1) includes a R^2 side chain with a vinyl terminus without α-methylation. The structural similarity of **1g** and **1h** complicated the purification of each compound. We were only able to obtain pure doscadenamide G (**1g**, Figure 1), and the ^{1}H NMR spectrum of **1g** in $CDCl_3$ indicated the presence of a vinyl group at 4.97 ppm. The HRESIMS spectrum of **1g** in positive mode shows a $[M + H]^+$ peak at m/z 445.3063 with eight degrees of unsaturation (Figure S29, Table S6). Due to the difficulty of purifying doscadenamide H (**1h**, Figure 1), we synthesized the compound with the proposed structure (Scheme 1) using our established synthetic route[9] and compared its ^{1}H NMR spectrum with the isolated fraction, confirming the dominant presence of doscadenamide H (**1h**) in the natural product fraction (Figure S30). The proposed doscadenamides I (**1i**) and J (**1j**) coeluted under various HPLC conditions and were present in roughly equal abundance (1:1 mixture). To confirm our hypothesis, we synthesized the two compounds, established the structures and compared their ^{1}H NMR spectra with the coeluting natural products, confirming their presence (Figure S31, Table S7).

Synthesis of a Strategic Focused Library to Probe the SAR. In addition to doscadenamides that are biosynthesized through natural diversification, we aimed to prepare a complementary compound set that possessed different degrees of methylation and/or unsaturation in the carboxylic acid chains (**1k**−**1n**), lacked one of the carboxylic acid chains (**2a**,**b** vs **3a**−**3c**), exhibited different pyrrolinone configuration (**1o**) or transposed pyrrolinone functionalization (**1p**), as well as a cyclized version (**4a**) (Figure 1). We termed these new synthetic analogues doscadenamides S4−S15 (Figure 1). The previously reported diastereomers of **1a** were named doscadenamides S1−S3 (Supporting Information, Figure S32).

To explore the contribution of each structural characteristic in doscadenamide A (**1a**, Figure 1) to the interaction with its target and its biological activity, we synthesized most of these structural analogues (doscadenamides F−J, **1f**−**1j**) following a similar approach as previously described[9] for **1a** and exemplified by the synthesis of doscadenamide H (**1h**, Scheme 1). Each target compound can be obtained in three main steps: pyrrolinone construction, carboxylic acid activation, and amide/imide coupling. For certain analogues (**1f**, **1k**, **1l**, **1m**, **2b**, **3b**, and **3c**), we synthesized additional carboxylic acids as specific building blocks to prepare the desired products. The detailed synthesis steps are described in the Supporting Information.

Our preliminary study indicated that the diastereomeric doscadenamides S1−S3 (Figure S32) behave similarly in modulating QS in *Pseudomonas aeruginosa*.[9] To perform the SAR study of doscadenamides systematically, we selected several analogues to compose a focused library for primary

https://dx.doi.org/10.1021/acs.jnatprod.0c01003
J. Nat. Prod. 2021, 84, 779−789

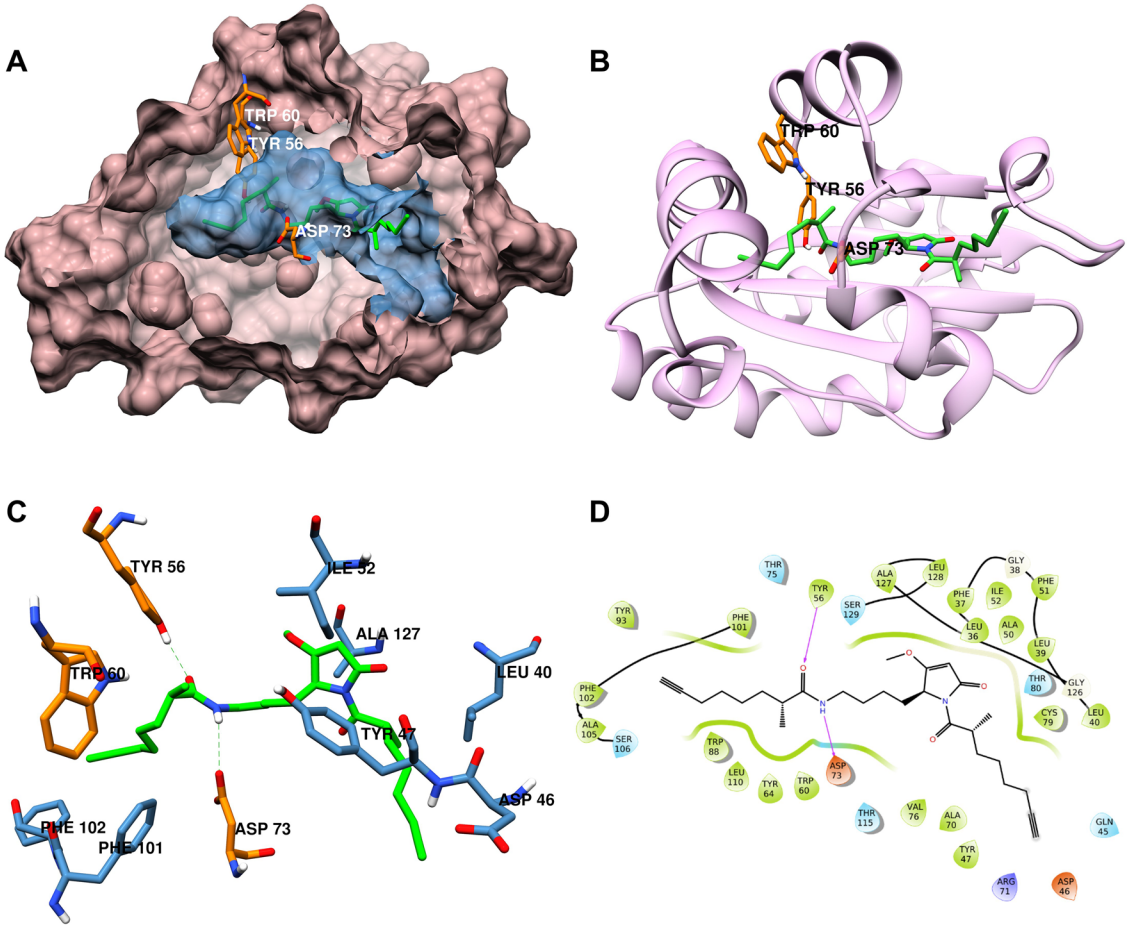

Figure 2. Docked structure of doscadenamide A into LasR pocket. (A) Image showing the protein surface, clipped to show the buried binding pocket (blue). (B) Cartoon diagram of the protein in the same orientation as in A. The mutated residues Tyr56, Trp60, and Asp73 are shown in orange. (C) Detailed view of the binding mode. The system is rotated to better show the interactions. (D) Ligand interaction diagram of the binding mode. Regions in green are hydrophobic, light blue are polar, red is negatively charged, and dark blue are positively charged. Purple arrows indicate hydrogen bonds. Numbering was adapted from the work of Zou et al.[13]

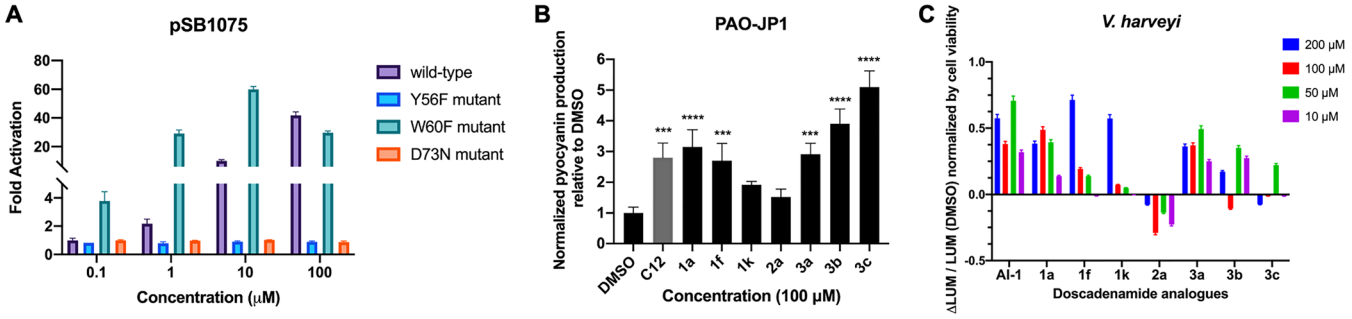

Figure 3. QS activity in different systems. (A) Activity of doscadenamide A (**1a**) in *E. coli* reporter gene assay using pSB1075 (wild-type) and point mutants (Y56F, W60F, and D73N). (B) Normalized pyocyanin production in *P. aeruginosa* mutant PAO-JP1 after treatment with doscadenamide A (**1a**) and its structural analogues for 6 h at 100 μM. C12 was used as the positive control. (C) Measurement of QS activating activity of doscadenamide A (**1a**) and its structural analogues in *V. harveyi* after 8 h treatment, presented by ΔLUM/LUM (DMSO) [ΔLUM = LUM(doscadenamide analogue) − LUM(DMSO)] normalized by cell viability measured with OD600. AI-1 is a reported quorum sensing autoinducer in this system (Figure S33) and was used as the positive control.

studies (Figure 1, highlighted in yellow). To explore the contribution of the unsaturated alkyne moiety to the bioactivity of doscadenamide A (**1a**, Figure 1), we included structural analogues with two unsaturated alkene termini (**1f**, Figure 1) and two saturated carboxylic acid moieties (**1k**, Figure 1). To further investigate the significance of each side chain in doscadenamides, we included structural analogues **2a** and **3a**−**3c**, possessing only one carboxylic acid chain and with different degrees of unsaturation. To confirm the previously hypothesized[9] importance of the linear structure of doscadenamide A (**1a**, Figure 1), the cyclic compound **4a** was also included in the library.

QS Modulation by Doscadenamides in *Pseudomonas aeruginosa* and LasR Molecular Interaction Studies. We

https://dx.doi.org/10.1021/acs.jnatprod.0c01003
J. Nat. Prod. 2021, 84, 779−789

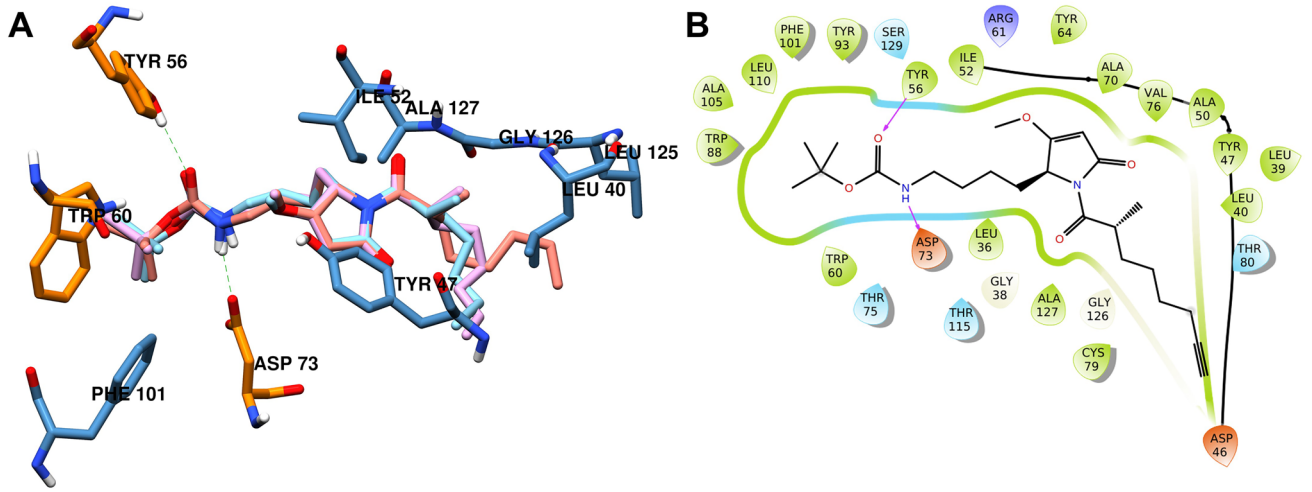

Figure 4. Three-dimensional representation of **3a**–**c** (A) in the binding pocket (**3a**, cyano; **3b**, pink; **3c**, orange), and diagram showing the interactions with the surrounding residues (B) for **3a**. Regions in green are hydrophobic, light blue are polar, red is negatively charged, and dark blue are positively charged. Purple arrows indicate hydrogen bonds. The binding modes of the other agonists (**3b**,**c**) are similar and are shown in Figure S36.

previously determined that doscadenamide A (**1a**) activates QS, which was established using the 3-oxo-C12-HSL-responsive reporter plasmid pSB1075,[12] a plasmid encoding LasR (the C12 HSL receptor in *Pseudomonas aeruginosa*) and containing a light-producing luxCDABE cassette expressed in *Escherichia coli*. The activity was abolished in a strain (pTIM5319) that lacked the AHL domain.

We first interrogated potential binding modes of doscadenamide A (**1a**). Figure 2A,B show the LasR protein highlighting the deep binding pocket with doscadenamide A in place. Figure 2C,D show a representative pose of the binding mode. Compared to the structure of LasR with the autoinducer *N*-3-oxo-dodecanoyl acyl homoserine lactone (C12, Figure S33), the interactions of the C12-polar headgroup are replaced by the amide bond in the doscadenamide A pyrrolinone-N side chain, which forms H-bonds to Tyr56 and Asp73 (Figure S34) (numbering for the protein following Zou and Nair[13]).

We screened three mutant strains (Y56F, W60F, and D73N) in our LasR reporter gene assay in *E. coli* to study the molecular interaction between doscadenamide A (**1a**, Figure 1) and LasR in concert with docking. The assay result (Figure 3A) indicated the strong binding contribution of the Tyr56 and Asp73 residues, consistent with molecular docking results (Figure 2C,D).

No bonds to Trp60 are formed. However, the acyl chain may form hydrophobic interactions with Trp88, Tyr93, and Phe101; the latter on the α5 helix. The pyrrolinone is buried deeper in the binding pocket, surrounded by Leu36, Gly38, Tyr47, Ala50, Ile52 Val76, and Ala127. Tyr47, in the L3 loop that closes the binding site, is in position to establish a side-to-face π interaction with the heterocycle. The pyrrolinone-N side chain extends further in the tunnel toward the right side of the figure, surrounded by Leu40, Asp46, Tyr47 (backbone), Arg71, and Thr80. Most of those interactions are the same as detected for the long hydrophobic tail in the autoinducer.

To follow up our previous study regarding the QS modulatory activity of doscadenamide A (**1a**) on wild-type *P. aeruginosa* and extend our reporter gene assay studies, we examined the QS activation of different doscadenamides using a QS systems deficient strain, PAO-JP1.[14] PAO-JP1 is a *P. aeruginosa* mutant with a *lasI* deletion that cannot produce C12.[15] To investigate the activating effect of doscadenamide A on *P. aeruginosa* without interference from the C12 produced by *P. aeruginosa* itself, we examined the pyocyanin production of *P. aeruginosa* mutant PAO-JP1 after treatment with doscadenamide A and selected structural analogues (Figure 1) for 6 h at 100 μM.

Compounds selected for this bioassay possessed a different number of carboxylic acid chains (**1a** vs **2a** vs **3a**) or different degrees of unsaturation (**1a**/**f**/**k** vs **3a**–**c**). As shown in Figure 3B, when normalized for cell number, these doscadenamides (Figure 1) can all activate the pyocyanin production of PAO-JP1 but to a different extent at the concentration of 100 μM. Doscadenamide A (**1a**) induced 3-fold QS activation, similarly to the positive control C12. Compound **2a**, which possesses only one side chain R^1, exhibits minimal QS-activating effect, while **3a**–**c** with acylation of the amide core showed the most potent activation, 3-fold, 4-fold, and 5-fold, indicating that this chain is predominantly responsible for the QS agonist activity in *P. aeruginosa*. The degree of unsaturation appears to play a minor role in a chain-dependent fashion, as the trends for **1a**/**f**/**k** vs **3a**–**c** were opposite, possibly indicating the dependence of both chains to the overall net effect. The overall trend was the same even without normalization for bacterial cell count (Figure S35), except that **2a** did not show any level of activation, further underscoring the critical importance of Moya2 (regardless of degree of saturation) for QS activation. Moreover, these results are consistent with our docking results, which suggest that unsaturation of doscadenamides would not obviously impact binding.

Thus, we focused on compounds **3a**–**3c** in our molecular analysis. Figure 4A shows representative docked poses for **3a**–**c**, and Figure 4B displays the binding mode of the agonist **3a** to LasR. The binding modes of the other agonists (**3b**,**c**) are similar and are shown in Figure S36. The amide bond in all those ligands make the same interactions as in **1a**, with the compound anchoring in pocket by the two H-bonds between Tyr56 and Asp73 and the Moya1 side chain, and the pyrrolinone surrounded by the same residues as in **1a**. Furthermore, in the agonist compounds, the Moya2 side chain extends toward the right side of the figure, similar to the

https://dx.doi.org/10.1021/acs.jnatprod.0c01003
J. Nat. Prod. 2021, 84, 779–789

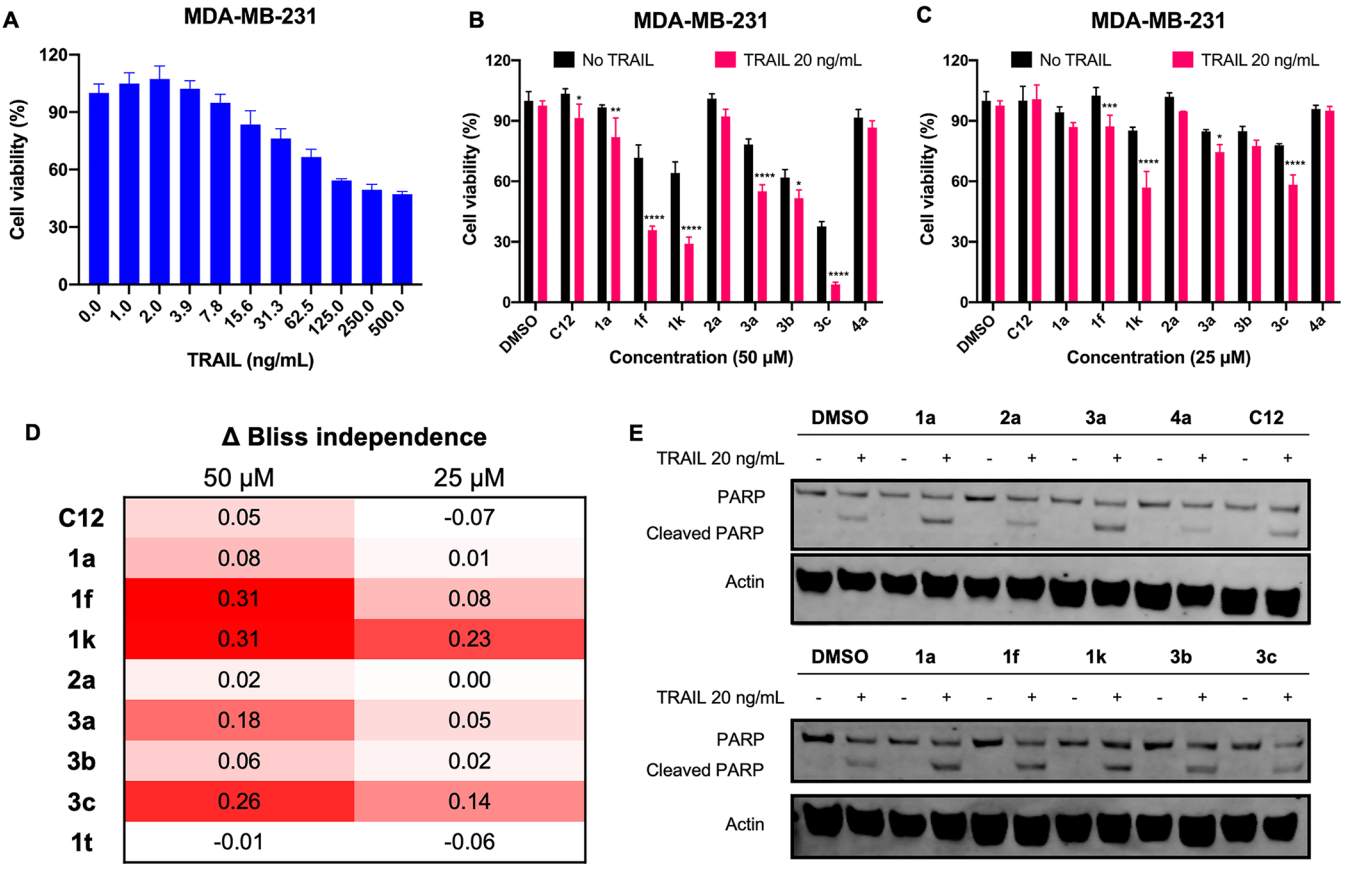

Figure 5. Doscadenamide A (**1a**) and its structural analogues sensitize breast cancer MDA-MB-231 cells in combination with TRAIL. (A) Dose–response analysis of TRAIL on MDA-MB-231 cells. (B, C) MDA-MB-231 cell viability after 3 h pretreatment with DMSO (solvent control), C12 or doscadenamides, at (B) 50 and (C) 25 μM, followed by combined TRAIL (20 ng/mL) treatment for 24 h. (D) Δ Bliss independence calculations for MDA-MB-231 cells cotreated with TRAIL (20 ng/mL) and doscadenamides. MDA-MB-231 cells were treated with doscadenamide A (**1a**) and its structural analogues for 3 h, followed by treatment with TRAIL (20 ng/mL) for 24 h, C12 was included as positive control. "Δ Bliss independence" is the difference between observed growth inhibition and Bliss expectation. Values greater than zero represent a synergistic response, represented by red highlights. Bliss expectation is $C = (A + B) - (A \times B)$, where A and B are the growth inhibition fractions of two compounds at a given dose. Cell viability was quantified using MTT assay. (E) A representative result of Western blot analysis of protein extracts from breast cancer MDA-MB-231 cells after treatment with TRAIL (20 ng/mL), doscadenamide A (**1a**), and selected analogues (50 μM) and their combinations as shown.

doscadenamide A case, establishing similar interactions with the L3 loop and stabilizing the protein. However, missing the N side chain, the antagonist **2a** is incapable of interacting with the L3 loop (Figure S37).

QS Modulation by Doscadenamides in other Gram-Negative Bacteria: *Vibrio harveyi*. We then aimed to determine if doscadenamides modulate QS in other Gram-negative bacteria. To extend our investigation of doscadenamides on QS modulation, we adopted a bioluminescent marine bacterium, *Vibrio harveyi*, as our model system to examine the effect of doscadenamides on modulating the bioluminescence production. *V. harveyi* has been reported to be responsive to bacterial QS activator *N*-(3-oxododecanoyl)-L-homoserine lactone (C12) and thus serves as a robust model for quorum sensing related research.[16,17]

Most Gram-negative bacteria possess QS circuits similar to the marine symbiotic bioluminescent bacterium *Vibrio fischeri*, the QS system which has been studied the most.[18] As the *V. fischeri* population grows, it produces and releases autoinducer molecules to accumulate and thus eliciting bioluminescence.[19] There are two proteins, LuxI and LuxR, in *V. fischeri* to regulate the QS signaling pathway. LuxI regulates the production of the autoinducer, *N*-(3-oxohexanoyl)-homoserine lactone (C6).[20] LuxR binds to the autoinducer and activates the transcription of luciferase enzymes for bioluminescence production.[21] In *P. aeruginosa*, two pairs of LuxI/LuxR homologues, namely LasI/LasR and RhlI/RhlR, exist to regulate the QS signaling pathway.[17] For these two signaling systems, the RhlI/RhlR system is subordinate to the LasI/LasR system.[21] Two acylhomoserine lactones (AHLs), C12 and *N*-butyryl-homoserine lactone (C4) (Figure S33) are required to trigger the expression of RhlR and its downstream target genes including virulence factor production, while the expression of LasR is independent of the AHL-mediated QS signaling pathway, thus making LasR a representive target for QS inhibition.[22] Compared to *V. fischeri* and *P. aeruginosa*, *V. harveyi* contains a more complex QS cascade involving three parallel regulating QS-signaling pathways and responds to three different autoinducers.[23,24] Even though the homologous LuxI/LuxR system of *V. fischeri* has never been identified in *V. harveyi*, *V. harveyi* can produce and detect autoinducer 1 (AI-1), *N*-(3-hydroxybutanoyl) homoserine lactone,[23] which shares significant similarity to C12 and C4 (Figure S33). More importantly, Tyr56 and Asp73 are conserved in both LasR and LuxR systems. Therefore, we adopted *V. harveyi* as a practical model

https://dx.doi.org/10.1021/acs.jnatprod.0c01003
J. Nat. Prod. 2021, 84, 779–789

to understand and validate the QS modulating activity of doscadenamide A (**1a**) and its analogues (Figure 1).

Almost all compounds activated QS in this biological context to a certain extent (Figure 3C), with **1a** and **3a** activating across the concentration range tested (10−200 μM). However, **3c** only had a minor activating trend and for **1f** and **1j** the activities at ≤100 μM were also reduced, suggesting that increased saturation of the terminal units decreases activity for both chains. Most notably, **2a** was not able to activate the bioluminescent response in *V. harveyi* but, instead, consistently inhibited QS signaling in *V. harveyi*, whereas the same compound was essentially inactive in *P. aeruginosa*. In both cases, **2a** was not able to activate QS, providing common ground in the two Gram-negative bacteria. The same trend in *V. harveyi* was observed without normalization for cell number (Figure S38), indicating that the differential effect is not an artifact of normalization.

These results indicate that both acylations in doscadenamide A are involved in the QS modulating activity, with partially overlapping but also bacteria-specific trends. Both chains contribute differently to the final biological activity output, even in opposing or interacting fashion, suggesting a more complex interaction between doscadenamide A and its molecular targets in various bacterial systems, potentially regulating their respective activity.

Synergy with TRAIL in MDA-MB-231 Breast Cancer Cells. TRAIL has been regarded as an attractive therapeutic anticancer agent; however, many cancer cells have developed resistance to TRAIL, impacting the treatment efficacy.[4] Given that C12 was reported to exhibit a synergistic effect on TRAIL-induced apoptosis in cancer cells,[7] we examined the potential synergistic effect of doscadenamide A (**1a**) and its analogues on sensitizing cancer cells. First, we generated the dose−response curve of TRAIL in MDA-MB-231 breast cancer cells, which were partially responsive to TRAIL. Cell viability remained 50% even at the highest concentration (500 ng/mL) after 24 h treatment (Figure 5A). A concentration of 20 ng/mL was selected, under which TRAIL would reduce cell viability by approximately 20% (Figure 5A). MDA-MB-231 cells were pretreated with C12, doscadenamides (25 or 50 μM) or solvent control for 3 h and then stimulated with TRAIL for 24 h (Figure 5B,C). Cell viability was measured and ΔBliss independence of each compound with TRAIL in a doscadenamide concentration-dependent manner calculated. Most analogues exhibited synergistic effect with TRAIL at 50 μM, except **2a** (Figure 1), and among all the analogues, the "saturated" analogues **1k** and **3c** (Figure 1) behaved as the best agents to sensitize MDA-MB-231 cells (Figure 5D). To further investigate the pro-apoptotic effect of doscadenamide A (**1a**, Figure 1), the poly(ADP-ribose) polymerase (PARP) cleavage was also analyzed using Western blot (Figure 5E) to indicate programmed cell death. The decrease in cell viability correlated with the presence of cleaved PARP in cell extracts after cotreatment, suggesting that doscadenamide A (**1a**, Figure 1) and its analogues can effectively improve TRAIL-induced apoptosis in MDA-MB-231 cells. Collectively, our SAR study revealed that low degrees of unsaturation lead to high potency of the analogues to ameliorate TRAIL resistance. Importantly, the R^2 side chain is more critical for the bioactivities of doscadenamide analogues than the R^1 side chain (Figure 1); **2a** showed no effect on cell viability (Figure 5B,C) or effect on PARP cleavage (Figure 5E). Compound **3c** showed enhanced activity compared with the doubly acylated versions, including the parent compound, doscadenamide A (**1a**). As expected, the cyclized version **4a** was completely inactive in these assays. Compared to doscadenamide A (**1a**), the analogues with lower unsaturation number (**1f**, **1k**, **3b**, and **3c**) not only performed better as synergistic agents with TRAIL but also exhibited inherent weak cytotoxic effects on MDA-MB-231 cells. This finding provides an approach to optimize doscadenamides with improved cytotoxic activities, although the active concentration is still relatively high.

DISCUSSION

Providing perspective of our findings, doscadenamides were isolated from a natural product "superproducer" with tremendous biosynthetic capability, *Moorena bouillonii* from Apra Harbor, Guam,[25] which previously yielded several apratoxins,[26−29] lyngbyabellins,[30−33] lyngbyalosides,[33,34] laingolide B,[33] apramides,[35,36] lyngbyastatin 2,[37] lyngbyapeptins,[32,33] and apratyramide.[38] The lipopeptides apramides possess partial structural similarity to doscadenamides. Doscadenamide A (**1a**) possesses two C8-alkynoic acid moieties (Moya) that are present in apramides[35] and several natural products from marine cyanobacteria, representing a biosynthetic signature motif.[35,39−43] Both units in doscadenamides appear to play complementary or opposing functions in different biological contexts, overall modulating the biological outcome. Similar to apramides A−G,[35] natural diversification by the cyanobacterial biosynthetic machinery is exemplified by the production of numerous additional doscadenamides (**B−J**, **1b−1j**) with minor structural changes that fine-tune bioactivities. To further diversify the doscadenamide family, structurally and functionally, we have developed a robust scheme to synthesize different structural and configurational doscadenamide analogues, including different degrees of unsaturation (**1k−n**, **2a−b**, **3a−c**). Notably, a related pyrrolinone core with two different pendant side chains is also the scaffold of the sponge-derived sintokamides, and natural and synthetic diversification has been reported[44,45] for this class of natural products.

The degree of terminal unsaturation in C_8 carboxylic acid chains has previously been demonstrated to modulate activity toward prokaryotic and eukaryotic cells. For instance, pitipeptolides A, D−F[39] (alkynoic side chain) and pitipeptolides B (alkenoic acid acid) and C (alkanoic acid chain) were reported to display differential cancer cytotoxic activity and antimycobacterial activity, depending on the degree of unsaturation. Both doscadenamides and pitipeptolides can be regarded as natural product examples that show that different degrees of unsaturation lead to fine-tuned biological activities.

We have shown that doscadenamides can modulate the quorum sensing signaling pathway in *P. aeruginosa*, acting as non-HSL inducers. An HSL-type QS inducer bearing a C8 (saturated) carboxylic acid (C8-HSL) has been previously identified from a cyanobacterium,[22,46,47] while other (particularly branched/substituted) cyanobacterial carboxylic acids or derivatives have usually been found to act as inhibitors of quorum sensing.[22] To further understand the molecular interaction of doscadenamide A and its bacterial receptor LasR in *P. aeruginosa*, we performed interactive mutation and molecular docking studies. Molecular docking is a powerful method to model the interactions between small molecules and proteins. There are, however, two main limitations that must be considered in such a study. The first limitation relates to the standard docking procedure where different conformations of

https://dx.doi.org/10.1021/acs.jnatprod.0c01003
J. Nat. Prod. 2021, 84, 779−789

the ligand are tested against the same structure of a rigid target whereas, in reality, the target may adjust to better accommodate each ligand. To circumvent this limitation, we included the effect of target flexibility by first using molecular dynamics to sample the conformational space of LasR, followed by clustering to select 15 different structures of the protein, to which the ligands were docked. Another important limitation is in the approximate nature of the scoring functions used, which are generally unable to reliably discriminate between ligand poses with similar binding energies. Here we collected all the structures within 3 kcal/mol of the lowest binding energy as reasonable structures, and selected the ones showing the interactions that were experimentally determined to be important.

We identified two amino acid residues in LasR from *P. aeruginosa* that play a critical role in binding with doscadenamide A and performed molecular modeling for further understanding of the binding mode between doscadenamides and LasR. The experimental mutagenesis results show that Tyr56 and Asp73 are required for the binding of **1a** to LasR. The selected docked structures confirm the importance of residues Tyr56 and Asp73 for ligand recognition, by establishing H-bonds to the atoms in the amide bond in the Moya1 side chain and anchoring the ligands. The docking results show very similar interaction patterns of these with all the ligands, indicating that these interactions must be important for ligand recognition, but not necessarily for activation. This is in agreement with Zou and Nair,[13] who concluded (based on the crystal structures) that activation is a result of the interactions of the long hydrophobic tail of the autoinducer with the residues of the L3 loop, which closes the active site and stabilizes LasR, allowing dimerization.[13] In agreement with this mechanism, the results show that the Moya2 side chains in the agonists **1a** and **3a**−**c** are able to establish the required interactions with the L3 loop to stabilize the structure and promote dimerization, activating LasR. On the other hand, the **2a** is still able to bind but, missing this side chain, is incapable of forming the necessary interactions to promote dimerization and activation (Figure S37).

The mutagenesis analysis here did not confirm the requirement of interactions to Trp60 for ligand binding, and the dockings show that none of the ligands considered here establish H-bonds to Trp60. The analysis did show, however, a dose-dependent effect on the W60F mutant. The Trp60 residue is located on the back of the binding pocket, and most of its contacts with the ligand are hydrophobic in nature. The MD simulations also show interactions of Trp60, which is located in the α3 helix, with residues in the opposed α5 helix (95−108), which stabilize the α5 helix. In the W60F mutant, both sides become more mobile. It was suggested that the local structure around Trp60 might be in contact with transcription factors and, thus, involved in the process of transcription-activation.[13] This increased flexibility of the binding site may be responsible for the slight increased response of the W60F mutant with respect to the WT by interfering with this mechanism. Finally, although these results agree with the experimental data on LasR, it is important to note that other factors that cannot be assessed by the techniques used here must play an important role, such as access to the binding site and neighbor interactions in the biological assembly. Furthermore, some of the experimental results here were obtained for a different system, *Vibrio harveyi*. Unfortunately, there is still not enough information about the receptor in this organism to build a reliable model. Nevertheless, we have confirmed that the Moya2 side chain plays an important role in the interactions of doscadenamides with LasR, largely contributing to the bioactivity in Gram-negative bacteria.

These compounds also have effects against mammalian cells, although the eukaryotic target remains to be determined. Importantly, the improved efficiency of TRAIL-induced apoptosis after pretreatment with doscadenamides would provide a new template to the development of therapeutic agents toward anticancer therapy to alleviate and overcome drug resistance. Sensitizing cancer cells to chemotherapy is an important concept to improve the therapeutic window of treatments.[48] We have shown that doscadenamides synergize with TRAIL, an inducer of the extrinsic apoptotic pathway.[49] The dual activity on QS and cancer cells reveal an interesting interplay of molecular pathways in bacteria and eukaryotes. Through total synthesis, we were able to discover new doscadenamide analogues to display improved anticancer activity, especially (or only) when combined with TRAIL. From a medicinal chemistry perspective, these analogues revealed a critical element to optimize the *in vitro* activity, although the potency is low and floppiness may hinder significant improvement. Nevertheless, cotreatment of doscadenamide-type agents and TRAIL may provide a template for a new treatment modality. On the other hand, doscadenamides with more potent cytotoxic activity were discovered through efficient total synthesis, which demonstrates our developed synthetic route as a robust approach to produce diverse analogues with various biological activities.[50]

EXPERIMENTAL SECTION

General Experimental Procedures. All commercial reagents were used without further purification unless otherwise noted. Flash column chromatography was performed with Fisher 170−400 mesh silica gel. NMR spectra were recorded on a Bruker Avance III 600 MHz spectrometer or a Bruker Avance Neo-600 spectrometer with a broadband Prodigy cryogenic probe. Chemical shifts for ^{1}H NMR spectra are reported in ppm relative to the signal residual $CDCl_3$ at 7.26 ppm. Chemicals shifts for ^{13}C NMR spectra are reported in ppm relative to the center line of the $CDCl_3$ triplet at 77.16 ppm. Optical rotation was measured on a PerkinElmer 341 polarimeter (Na D line) using a microcell of 1 dm path length. HRMS was conducted using a Thermo Fisher Q Exactive Focus mass spectrometer.

Biological Material. The cyanobacterium *Moorena bouillonii*[25] was collected in May 2005 by SCUBA in shallow waters at Finger Reef, Apra Harbor, Guam. This is a recollection of VP417 (16S rRNA gene sequence deposited under GenBank accession nos. AY049750 and AY049751)[27] and previously yielded doscadenamide A.[9] A voucher specimen is located at the Smithsonian Marine Station.

Extraction and Isolation. The sample was extracted with CH_2Cl_2 and MeOH (2:1) and the extract (10 g) was fractionated using column chromatography on silica gel, eluting with CH_2Cl_2 containing increasing concentrations of iPrOH to afford 16 fractions. Fractions 3, 4, and 5 (2% iPrOH in CH_2Cl_2; 400 mg, 1.54 g, and 100 mg) and fractions 6 (5% iPrOH in CH_2Cl_2; 71 mg) were individually subjected to semipreparative HPLC (Phenomenex Phenyl-hexyl, 250 × 10 mm, 5 μ, 2.0 mL/min; PDA detection) using a MeOH−H_2O linear gradient (90−100% MeOH in 30 min and 100% MeOH for 10 min). Fractions were pooled based on retention times, ^{1}H NMR analysis, and low-resolution MS measurements to afford impure doscadenamide A (**1a**) containing fractions. These fractions were further purified with HPLC (Ultracarb, 250 × 10 mm, 5 μ, 2.0 mL/min; PDA detection) using a MeOH−H_2O linear gradient (90−100% MeOH in 30 min and 100% MeOH for 10 min) to afford a series of compounds (**1a**, 4.5 mg, t_R = 11.0 min; **1b**, 0.3 mg, t_R = 10.0 min; **1c**, 0.3 mg, t_R =

https://dx.doi.org/10.1021/acs.jnatprod.0c01003
J. Nat. Prod. 2021, 84, 779−789

13.7 min; **1d**, 0.5 mg, t_R = 14.7 min; **1e**, 0.2 mg, t_R = 11.9 min; **1f**, 0.2 mg, t_R = 13.9 min; **1g**, 0.3 mg, t_R = 12.4 min; **1h**, present in a mixture, 0.2 mg, t_R = 12.6 min; **1i**/**1j**, binary mixture, 0.6 mg, t_R = 9.4 min).

*Doscadenamide A (**1a**).* White solid; $[\alpha]^{20}_D$ + 40 (*c* 0.07, MeOH)].[9]

*Doscadenamide B (**1b**).* White solid; $[\alpha]^{20}_D$ + 127 (*c* 0.05, MeOH); ^{1}H and ^{13}C NMR data, see Table S1; HRESIMS *m*/*z* [M + H]$^+$ 455.2897 (calcd for $C_{27}H_{39}N_2O_4$, 455.2904).

*Doscadenamide C (**1c**).* White solid; $[\alpha]^{20}_D$ + 116 (*c* 0.02, MeOH); ^{1}H and ^{13}C NMR data, see Table S2; HRESIMS *m*/*z* [M + H]$^+$ 459.3218 (calcd for $C_{27}H_{43}N_2O_4$, 459.3217).

*Doscadenamide D (**1d**).* White solid; $[\alpha]^{20}_D$ + 118 (*c* 0.03, MeOH); ^{1}H and ^{13}C NMR data, see Table S3; HRESIMS *m*/*z* [M + H]$^+$ 459.3226 (calcd for $C_{27}H_{43}N_2O_4$, 459.3217).

*Doscadenamide E (**1e**).* White solid; $[\alpha]^{20}_D$ + 115 (*c* 0.02, MeOH); ^{1}H and ^{13}C NMR data, see Table S4; HRESIMS *m*/*z* [M + H]$^+$ 445.3069 (calcd for $C_{26}H_{41}N_2O_4$, 445.3061).

*Doscadenamide F (**1f**).* White solid; $[\alpha]^{20}_D$ + 114 (*c* 0.03, MeOH); ^{1}H and ^{13}C NMR data, see Table S5; HRESIMS *m*/*z* [M + H]$^+$ 461.3362 (calcd for $C_{27}H_{45}N_2O_4$, 461.3374).

*Doscadenamide G (**1g**).* White solid; $[\alpha]^{20}_D$ + 110 (*c* 0.06, MeOH); ^{1}H and ^{13}C NMR data, see Table S6; HRESIMS *m*/*z* [M + H]$^+$ 445.3063, (calcd for $C_{26}H_{41}N_2O_4$, 445.3061).

*Doscadenamide H (**1h**).* White solid; HRESIMS *m*/*z* [M + H]$^+$ 445.3063, (calcd for $C_{26}H_{41}N_2O_4$, 445.3061).

*Doscadenamide I/J (**1i**/**1j**).* White solid; ^{1}H and ^{13}C NMR data, see Table S7; HRESIMS *m*/*z* [M + H]$^+$ 443.2916, (calcd for $C_{26}H_{39}N_2O_4$, 443.2910).

Quorum Sensing Reporter Assays with Doscadenamide A (1a). **1a**, in a dose−response manner, and EtOH control were added to the corresponding wells in a 96-well plate and the solvent was allowed to evaporate. Then 100 μL of an overnight culture of *E. coli* expressing plasmid wild-type pSB1075 (a *luxCDABE* reporter construct encoding LasR) or an overnight *E. coli* culture expressing reporter pSB1075 mutant (Y56F, W60F or D73N; obtained from Dr. Max Teplitski, UF), was added to each well. The plate was incubated at 37 °C for 6 h before the measurement of luminescence.

Pyocyanin Quantification in *P. aeruginosa* Strain PAO-JP1. An overnight culture of *P. aeruginosa* strain PAO-JP1 (obtained from Dr. Everett C. Pesci, Department of Microbiology and Immunology, Brody School of Medicine, East Carolina University, and Dr. Abdul Hamood, Department of Surgery and Immunology and Molecular Microbiology, School of Medicine, Texas Tech University Health Science Center) was diluted 10-fold before being transferred to another culture tube containing 890 μL LB broth and 10 μL testing compound (10 μM final concentration) or EtOH control and incubated at 37 °C with shaking for 6 h. The culture was then spun down for 10 min at the maximum speed, and the supernatant was collected and filtered using 0.2 μM Eppendorf filters. A 500 μL portion of the sterile supernatant was added to 500 μL $CHCl_3$ in an Eppendorf tube. Tube shaking allowed for the extraction of pyocyanin in the $CHCl_3$ layer. This layer was then added to 150 μL of 0.2 N HCl in another Eppendorf tube. After shaking, the aqueous layer and the organic layer were separated. A 100 μL portion of the aqueous layer was transferred to a clear bottomed 384-well plate, and the absorbance was measured at 385 nm to quantify the pyocyanin production. Data was analyzed using GraphPad Prism 5 software.

Bioluminescence Modulation in *V. harveyi*. Bioluminescent *V. harveyi* BB120 strain (wild-type, obtained from Dr. Julie L. Meyer, Soil and Water Sciences Department, Institute of Food and Agricultural Sciences, University of Florida) was cultivated in AB media overnight (15−16 h) at 30 °C (OD600 2.0−2.5). The overnight cultivated strain (2 μL) was diluted to 10 mL by AB media (OD600 < 0.1). A 100 μL portion of the diluted BB120 strain was distributed to each well of 96-well white plate. The solution of each tested compound in DMSO (0.5 μL) at different concentrations was added to BB120 cultures on plate. Triplicate analysis was conducted for each compound and each concentration. After addition, bacterial cultures were incubated at 30 °C for 7 h. Then, the emitted luminescence and OD600 was measured on a SpectraMax M5 plate reader. AI-1 and DMSO were used as positive control and negative control, respectively.

Synergistic Effect Evaluation of Doscadenamide Analogues with TRAIL. MDA-MB-231 cells were seeded in 12-well plates at a density of 100 000 cells per well. The next day, cells were pretreated with doscadenamide analogues (50 μM and 25 μM), positive controls (C12, 50 μM) or solvent control (DMSO) for 3 h. Then the cells were treated with TRAIL (20 ng/mL) for 24 h. The whole cell lysates were collected using PhosphoSafe Buffer (EMD Chemicals). Protein concentrations were measured with the BCA Protein Assay kit (Thermo Fisher Scientific). Lysates containing equal amounts of protein were separated by NuPAGE 4−12% Bis-Tris protein gels (Thermo Fisher Scientific), transferred to polyvinylidene difluoride membranes, probed with primary and secondary antibodies. The membranes were visualized using Li-Cor imaging system. PARP and actin antibodies were from Cell Signaling. Secondary mouse and rabbit antibodies were from Invitrogen.

Ensemble Docking to LasR. The initial structure for LasR was obtained from its crystal structure in complex with the autoinducer mimic TP1 (PDBID: 3IX4), obtained at 1.8 Å resolution.[13] The protonation states of histidines were determined by the H++ server at pH 7.3 (http://biophysics.cs.vt.edu/H++).[51] Mutants were obtained by mutating the corresponding residue in the PDB file before preparing the system.

All MD calculations used a similar protocol with the programs from the AMBER18 suite.[52] The protein was neutralized by adding 7 Na^+ ions and placed in an octahedral box with 7405 TIP3P water molecules, ensuring a minimal distance of 10 Å between the protein atoms and the box limits. The system was then submitted to two stages of energy minimization. First, only water molecules were allowed to move for 100 steps. Then all atoms were allowed to move for 10 000 minimization steps. After that the system was heated from 0 to 310 K during 600 ps at constant volume, then kept at the final temperature for an extra 400 ps. This was followed by 2 ns equilibration at 310 K and constant pressure with the Monte Carlo barostat and 2 ps relaxation time. Finally, data was acquired during two 100 ns runs with the same conditions (total 200 ns production). All MD runs used a Langevin thermostat with collision frequency of 2.0 ps^{-1}, a 2 fs time step, and a 10 Å cutoff for nonbonded interactions. The trajectory obtained from the last 200 ns of simulation was split into 15 clusters using a hierarchical agglomerative algorithm, based on the root-mean-square distance between the frames, considering only the residues around the binding site, with the program CPPTRAJ, part of the AMBER18 suite. For each cluster, a representative structure was selected as the structure with the lowest cumulative distance to all other frames in the same cluster. All the input files used are in the Supporting Information.

All dockings were done in triplicate with AutoDock Vina 4.2,[53] with exhaustiveness of 128 and a grid box of dimensions 18.75, 24.375, and 18.75 Å (*x*, *y*, *z*), centered on the binding site. Results were analyzed using a combination of UCSF Chimera,[54] Jupyter notebooks (Python), and in-house scripts, available at GitHub. (https://github.com/gmseabra/lasr). Only poses within 3 kcal/mol from the pose with lowest Vina score in each case were considered. The final poses shown were selected to display the experimentally validated interactions.

■ ASSOCIATED CONTENT

Supporting Information

The Supporting Information is available free of charge at https://pubs.acs.org/doi/10.1021/acs.jnatprod.0c01003.

Experimental details of the chemical synthesis, Tables S1−7, and Figures S1−107, including NMR spectra and assay data (PDF)

https://dx.doi.org/10.1021/acs.jnatprod.0c01003
J. Nat. Prod. 2021, 84, 779−789

AUTHOR INFORMATION

Corresponding Author

Hendrik Luesch − *Department of Medicinal Chemistry and Center for Natural Products, Drug Discovery and Development (CNPD3), University of Florida, Gainesville, Florida 32610, United States;* orcid.org/0000-0002-4091-7492; Email: luesch@cop.ufl.edu

Authors

Xiao Liang − *Department of Medicinal Chemistry and Center for Natural Products, Drug Discovery and Development (CNPD3), University of Florida, Gainesville, Florida 32610, United States*

Qi-Yin Chen − *Department of Medicinal Chemistry and Center for Natural Products, Drug Discovery and Development (CNPD3), University of Florida, Gainesville, Florida 32610, United States*

Gustavo M. Seabra − *Department of Medicinal Chemistry and Center for Natural Products, Drug Discovery and Development (CNPD3), University of Florida, Gainesville, Florida 32610, United States;* orcid.org/0000-0002-1303-4483

Susan Matthew − *Department of Medicinal Chemistry, University of Florida, Gainesville, Florida 32610, United States*

Jason C. Kwan − *Department of Medicinal Chemistry, University of Florida, Gainesville, Florida 32610, United States*

Chenglong Li − *Department of Medicinal Chemistry and Center for Natural Products, Drug Discovery and Development (CNPD3), University of Florida, Gainesville, Florida 32610, United States*

Valerie J. Paul − *Smithsonian Marine Station, Fort Pierce, Florida 34949, United States;* orcid.org/0000-0002-4691-1569

Complete contact information is available at: https://pubs.acs.org/10.1021/acs.jnatprod.0c01003

Author Contributions

X.L.: total synthesis, biological experiments with MDA-MB-231, experimental design, and manuscript writing. Q.-Y.C.: supervision of total synthesis and biological experiments with PAO-JP1 and *V. harveyi*. G.M.S.: molecular docking. S.M.: isolation and structure elucidation. J.C.K.: biological evaluation using reporter assays. C.L.: supervision of molecular docking. V.J.P.: sample collection and identification and manuscript editing. H.L.: project supervision, experimental design, and manuscript editing. All authors have given approval to the final version of the manuscript.

Notes

The authors declare the following competing financial interest(s): The University of Florida has filed a patent application related to the subject of the manuscript.

ACKNOWLEDGMENTS

We acknowledge financial support from the National Institutes of Health (National Cancer Institute grant R01CA172310) and the Debbie and Sylvia DeSantis Chair professorship (H.L.). We thank Dr. Max Teplitski and Dr. Julie Meyer (Soil and Water Sciences Department, Institute of Food and Agricultural Sciences, University of Florida) for providing *E. coli* reporter and *V. harveyi* strains and support with the reporter assays. We also thank Dr. Everett C. Pesci (Department of Microbiology and Immunology, Brody School of Medicine, East Carolina University) and Dr. Abdul Hamood (Department of Surgery and Immunology and Molecular Microbiology, School of Medicine, Texas Tech University Health Science Center) for providing the PAO-JP1 strains.

DEDICATION

Dedicated to Dr. A. Douglas Kinghorn, The Ohio State University, for his pioneering work on bioactive natural products.

REFERENCES

(1) von Karstedt, S.; Montinaro, A.; Walczak, H. *Nat. Rev. Cancer* **2017**, *17*, 352−366.
(2) Srivastava, R. K. *Neoplasia* **2001**, *3*, 535−546.
(3) French, L.; Tschopp, J. *Nat. Med.* **1999**, *5*, 146−147.
(4) Trivedi, R.; Mishra, D. P. *Front. Oncol.* **2015**, *5*, 69.
(5) Amarante-Mendes, G.; Griffith, T. *Pharmacol. Ther.* **2015**, *155*, 117−131.
(6) Legler, K.; Hauser, C.; Egberts, J. H.; Willms, A.; Heneweer, C.; Boretius, S.; Röcken, C.; Glüer, C. C.; Becker, T.; Kluge, M.; Hill, O.; Gieffers, C.; Fricke, H.; Kalthoff, H.; Lemke, J.; Trauzold, A. *Cell Death Dis.* **2018**, *9*, 445.
(7) Kravchenko, V.; Garner, A. L.; Mathison, J.; Seit-Nebi, A.; Yu, J.; Gileva, I. P.; Ulevitch, R.; Janda, K. D. *ACS Chem. Biol.* **2013**, *8*, 1117−1120.
(8) The Spanish historic influence on the collection site Guam coupled with the structural features, the acylation with two ("dos") carboxylic acid chains ("cadenas") to form the final amide, led us to coin the name of this compound class.
(9) Liang, X.; Matthew, S.; Chen, Q. Y.; Kwan, J. C.; Paul, V. J.; Luesch, H. *Org. Lett.* **2019**, *21*, 7274−7278.
(10) Kiratisin, P.; Tucker, K. D.; Passador, L. *J. Bacteriol.* **2002**, *184*, 4912−4919.
(11) Swartzman, E.; Silverman, M.; Meighen, E. A. *J. Bacteriol.* **1992**, *174*, 7490−7493.
(12) Winson, M. K.; Swift, S.; Fish, L.; Throup, J. P.; Jørgensen, F.; Chhabra, S. R.; Bycroft, B. W.; Williams, P.; Stewart, G. S. *FEMS Microbiol. Lett.* **1998**, *163*, 185−192.
(13) Zou, Y.; Nair, S. K. *Chem. Biol.* **2009**, *16*, 961−970.
(14) Zhao, J.; Jiang, H.; Cheng, W.; Wu, J.; Zhao, J.; Wang, J.; Dong, L. *J. Basic Microbiol.* **2015**, *55*, 671−678.
(15) Smith, R. S.; Harris, S. G.; Phipps, R.; Iglewski, B. *J. Bacteriol.* **2002**, *184*, 1132−1139.
(16) Aharoni, R.; Bronstheyn, M.; Jabbour, A.; Zaks, B.; Srebnik, M.; Steinberg, D. *Bioorg. Med. Chem.* **2008**, *16*, 1596−1604.
(17) Naik, S. P.; Scholin, J.; Ching, S.; Chi, F.; Herpfer, M. *J. Agric. Food Chem.* **2018**, *66*, 40−44.
(18) Miller, M.; Bassler, B. *Annu. Rev. Microbiol.* **2001**, *55*, 165−199.
(19) Engebrecht, J.; Nealson, K.; Silverman, M. *Cell* **1983**, *32*, 773−781.
(20) Eberhard, A.; Burlingame, A. L.; Eberhard, C.; Kenyon, G. L.; Nealson, K. H.; Oppenheimer, N. J. *Biochemistry* **1981**, *20*, 2444−2449.
(21) Engebrecht, J.; Silverman, M. *Proc. Natl. Acad. Sci. U. S. A.* **1984**, *81*, 4154−4158.
(22) Kwan, J. C.; Meickle, T.; Ladwa, D.; Teplitski, M.; Paul, V.; Luesch, H. *Mol. BioSyst.* **2011**, *7*, 1205−1216.
(23) Henke, J. M.; Bassler, B. L. *J. Bacteriol.* **2004**, *186*, 6902−6914.
(24) Waters, C. M.; Bassler, B. L. *Genes Dev.* **2006**, *20*, 2754−2767.
(25) Tronholm, A.; Engene, N. *Notulae Algarum* **2019**, *122*, 1−2.
(26) Luesch, H.; Yoshida, W. Y.; Moore, R. E.; Paul, V. J.; Corbett, T. H. *J. Am. Chem. Soc.* **2001**, *123*, 5418−5423.
(27) Luesch, H.; Yoshida, W. Y.; Moore, R. E.; Paul, V. J. *Bioorg. Med. Chem.* **2002**, *10*, 1973−1978.

(28) Matthew, S.; Schupp, P. J.; Luesch, H. *J. Nat. Prod.* **2008**, *71*, 1113−1116.
(29) Wu, P.; Cai, W.; Chen, Q. Y.; Xu, S.; Yin, R.; Li, Y.; Zhang, W.; Luesch, H. *Org. Lett.* **2016**, *18*, 5400−5403.
(30) Luesch, H.; Yoshida, W. Y.; Moore, R. E.; Paul, V. J.; Mooberry, S. L. *J. Nat. Prod.* **2000**, *63*, 611−615.
(31) Luesch, H.; Yoshida, W. Y.; Moore, R. E.; Paul, V. J. *J. Nat. Prod.* **2000**, *63*, 1437−1439.
(32) Luesch, H.; Yoshida, W. Y.; Moore, R. E.; Paul, V. J. *Tetrahedron* **2002**, *58*, 7959−7966.
(33) Matthew, S.; Salvador, L. A.; Schupp, P. J.; Paul, V. J.; Luesch, H. *J. Nat. Prod.* **2010**, *73*, 1544−1552.
(34) Chang, C. F.; Stefan, E.; Taylor, R. E. *Chem. - Eur. J.* **2015**, *21*, 10681−10686.
(35) Luesch, H.; Yoshida, W. Y.; Moore, R. E.; Paul, V. J. *J. Nat. Prod.* **2000**, *63*, 1106−1112.
(36) Williams, P. G.; Luesch, H.; Yoshida, W. Y.; Moore, R. E.; Paul, V. J. *J. Nat. Prod.* **2003**, *66*, 595−598.
(37) Luesch, H.; Yoshida, W. Y.; Moore, R. E.; Paul, V. J. *J. Nat. Prod.* **1999**, *62*, 1702−1706.
(38) Cai, W.; Salvador-Reyes, L. A.; Zhang, W.; Chen, Q. Y.; Matthew, S.; Ratnayake, R.; Seo, S. J.; Dolles, S.; Gibson, D. J.; Paul, V. J.; Luesch, H. *ACS Chem. Biol.* **2018**, *13*, 91−99.
(39) Montaser, R.; Paul, V. J.; Luesch, H. *Phytochemistry* **2011**, *72*, 2068−2074.
(40) Salvador, L. A.; Biggs, J. S.; Paul, V. J.; Luesch, H. *J. Nat. Prod.* **2011**, *74*, 917−927.
(41) Mevers, E.; Liu, W. T.; Engene, N.; Mohimani, H.; Byrum, T.; Pevzner, P. A.; Dorrestein, P. C.; Spadafora, C.; Gerwick, W. H. *J. Nat. Prod.* **2011**, *74*, 928−936.
(42) Gunasekera, S. P.; Ross, C.; Paul, V. J.; Matthew, S.; Luesch, H. *J. Nat. Prod.* **2008**, *71*, 887−890.
(43) Gunasekera, S. P.; Owle, C. S.; Montaser, R.; Luesch, H.; Paul, V. J. *J. Nat. Prod.* **2011**, *74*, 871−876.
(44) Sadar, M. D.; Williams, D. E.; Mawji, N. R.; Patrick, B. O.; Wikanta, T.; Chasanah, E.; Irianto, H. E.; Soest, R. V.; Andersen, R. J. *Org. Lett.* **2008**, *10*, 4947−4950.
(45) Yan, L.; Banuelos, C. A.; Mawji, N. R.; Patrick, B. O.; Sadar, M. D.; Andersen, R. J. *J. Nat. Prod.* **2020**, DOI: 10.1021/acs.jnatprod.0c00921.
(46) Sharif, D. I.; Gallon, J.; Smith, C. J.; Dudley, E. *ISME J.* **2008**, *2*, 1171−1182.
(47) Kwan, J. C.; Teplitski, M.; Gunasekera, S. P.; Paul, V. J.; Luesch, H. *J. Nat. Prod.* **2010**, *73*, 463−466.
(48) Leary, M.; Heerboth, S.; Lapinska, K.; Sarkar, S. *Cancers* **2018**, *10*, 483.
(49) Sp, N.; Kang, D. Y.; Kim, D. H.; Yoo, J. S.; Jo, E. S.; Rugamba, A.; Jang, K. J.; Yang, Y. M. *Anticancer Res.* **2020**, *40*, 3209−3220.
(50) (a) While the manuscript was under review, doscadenamide A was also described from other *M. bouillonii* collections by Leber et al.[50b] In that paper, structures of doscadenamide analogues (nomenclature "B−J") were proposed merely based on low-resolution MS^2 fragmentation data, without isolation and rigorous structural analysis. These cannot be seriously considered as characterized natural products and remain hypothetical, so we did not take them into consideration. Our nomenclature (Figure 1) is also consistent with the patent literature: PCT/US2020/043495 (priority to July 26, 2019). (b) Leber, C. A.; Naman, C. B.; Keller, L.; Almaliti, J.; Caro-Diaz, E. J. E.; Glukhov, E.; Joseph, V.; Sajeevan, T. P.; Reyes, A. J.; Biggs, J. S.; Li, T.; Yuan, Y.; He, S.; Yan, X.; Gerwick, W. H. *Mar. Drugs* **2020**, *18*, 515.
(51) Anandakrishnan, R.; Aguilar, B.; Onufriev, A. V. *Nucleic Acids Res.* **2012**, *40* (Web Serverissue), W537−W541.
(52) Case, D. A.; Ben-Shalom, I. Y.; Brozell, S. R.; Cerutti, D. S.; Cheatham, I. T. E.; Cruzeiro, V. W. D.; Darden, T. A.; Duke, R. E.; Ghoreishi, D.; Gilson, M. K.; Gohlke, H.; Goetz, A. W.; Harris, R.; Homeyer, N.; Izadi, S.; Kovalenko, A.; Kurtzma, T.; Lee, T. S.; LeGrand, S.; Li, P.; Lin, C.; Liu, J.; Luchko, T.; Luo, R.; Mermelstein, D. J.; Merz, K. M.; Miao, Y.; Monard, G.; Nguyen, C.; Nguyen, H.; Omelyan, I.; Onufriev, A.; Pan, F.; Qi, R.; Roe, D. R.; Roitberg, A.; Sagui, C.; Schott-Verdugo, S.; Shen, J.; Simmerling, C. L.; Smith, J.; Salomon-Ferrer, R.; Swails, J.; Walker, R. C.; Wang, J.; Wei, H.; Wolf, R. M.; W, X.; Xiao, L.; York, D. M.; Kollman, P. A. *Amber18 / AmberTools18*; University of California: San Francisco, 2018.
(53) Trott, O.; Olson, A. J. *J. Comput. Chem.* **2009**, *31*, 455−461.
(54) Pettersen, E. F.; Goddard, T. D.; Huang, C. C.; Couch, G. S.; Greenblatt, D. M.; Meng, E. C.; Ferrin, T. E. *J. Comput. Chem.* **2004**, *25*, 1605−1612.

NOTE ADDED AFTER ASAP PUBLICATION

This paper was published ASAP on January 22, 2021, with a compound naming error in the Abstract text and in a Results heading. The corrected version was reposted on March 3, 2021.

https://dx.doi.org/10.1021/acs.jnatprod.0c01003
J. Nat. Prod. 2021, 84, 779−789